Editors' Suggestion

First-Principles Calculations of Shallow Acceptor-Carbon Complexes in Si: A Potential-Patching Method with a Hybrid-Functional Correction

Jun Kang[1,*] and Lin-Wang Wang[2]

[1] *Beijing Computational Science Research Center, Beijing 100193, China*

[2] *State Key Laboratory of Superlattices and Microstructures, Institute of Semiconductors, Chinese Academy of Sciences, P. O. Box 912, Beijing 100083, China*

(Received 22 September 2022; revised 12 October 2022; accepted 18 October 2022; published 1 December 2022)

Accurate modeling of shallow impurities in semiconductors through first-principles density-functional-theory calculations is challenging due to the delocalized nature of the impurity wave function. The situation could be more complicated for shallow impurity complexes where the interactions between impurities lead to a large perturbation to the host. In this work, the shallow acceptor levels of the group-IIIA acceptor-carbon (A-C, with A=B, Al, Ga, In, Tl) complexes in silicon are studied using a potential-patching method combined with a hybrid-functional correction. The potential-patching method removes the artificial interaction between periodic images and allows the calculations of large supercells containing over 10^4 atoms to obtain converged acceptor levels. The correction based on hybrid-functional calculations overcomes the underestimation of the ionization energies predicted by semilocal exchange-correlation functionals, resulting in good agreements with experiments. The A-C complexes are found to have smaller acceptor ionization energies than the corresponding single-A substitutional acceptors. The origin of the ionization energy reduction is further analyzed, and the roles of the chemical electronic effect and the strain-field effect are clarified. Our results indicate that the combination of the potential-patching method and the hybrid-functional correction could be a feasible approach for accurate simulations of shallow impurities and their complexes.

DOI: 10.1103/PhysRevApplied.18.064001

I. INTRODUCTION

In doped semiconductors, it is possible that several of the impurities occupy neighboring lattice sites, forming impurity complexes [1–5]. The interactions between impurities bring abundant doping effects, either desired or unwanted, which play a critical role in determining the performance of semiconductor devices by affecting impurity levels, carrier lifetimes, degradation, etc. Besides various experimental techniques, theoretical modeling of impurity complexes is helpful in understanding their properties and controlling their effects. In practice, deep impurity complexes, which have localized wave functions can be quite well described by the defect formation energy theory based on first-principles density-functional-theory (DFT) calculations with the supercell approach [6,7]. However, if the impurity complex is shallow, the impurity wave function is delocalized and can extend into thousands of atoms [8]. This is orders of magnitude larger than the typical supercell size in DFT calculations, therefore it is difficult to treat shallow impurities directly with conventional DFT methods.

A widely adopted approach to model shallow impurities is the effective mass approximation (EMA) [9], in which a central-cell correction depending on empirical parameters must be introduced to reproduce the chemical shift of different impurities [10,11]. Compared to single-atom impurities, EMA modeling of impurity complexes could rely more heavily on empirical parameters since the impurity-impurity interactions result in a larger perturbation to the host material, leading to more significant central-cell effects. Given the limited predictive power of EMA due to the use of empirical parameters, first-principles DFT approaches to model shallow impurity complexes are highly desirable.

In recent years, much progress has been made on DFT simulations of shallow impurities. Green's function approach combined with DFT calculations has been demonstrated to be able to accurately predict hyperfine interactions of shallow impurities [12,13], but this approach is not as straightforward as the supercell approach. In another approach, the shallow impurity wave function in a large supercell is first obtained from DFT calculations, and then perturbative calculations with an impurity potential are performed [14,15]. This procedure yields accurate impurity levels. However, it employs an

*jkang@csrc.ac.cn

empirical model to describe the impurity potential, and it is difficult to find a generalized model suitable for various impurity complexes. An extrapolation method with hybrid and semilocal functionals working in tandem is also proposed, and it well reproduces experimental ionization energies and hyperfine parameters of shallow group-V dopants P, As, and Bi in silicon [16,17]. Nevertheless, a supercell with a considerable size may still be necessary to obtain the correct scaling law. Plus, the exponential tail of the impurity wave function cannot be well captured with the relatively small supercell used for the extrapolation.

Converged shallow impurity levels and wave functions can be obtained by a DFT-based potential-patching method [8]. It removes the artificial interaction between periodic images and allows the calculations of large supercells containing over 10^4 atoms, but there is still an issue of ionization energy underestimation due to the failure of DFT eigenvalues to approximate quasiparticle energies [8]. A correction scheme to the potential-patching method based on *GW* calculations is then proposed, and the resulting impurity ionization energies are in excellent agreements with experiments [18]. However, in practice, *GW* calculations are usually carried out with supercells less than 10^2 atoms because of their high computational costs. Although this size could be enough to capture the character of the central-cell potential of a single dopant [18], it could be too small for impurity complexes where there are larger structural relaxation, making it challenging to apply the *GW* correction. Considering that the hybrid functionals, which mix a portion of exact exchange energy into the semilocal exchange-correlation functionals, satisfy the generalized Koopmans' condition [19] fairly well, one can expect that the hybrid functional eigenenergies could be a reasonable approximation to the quasiparticle energies. Therefore, it is possible to perform the computationally cheaper hybrid functional calculations instead of the *GW* calculations to apply the quasiparticle correction to the potential-patching method.

In this work, we justify the above proposal by taking the group-IIIA acceptor-carbon complexes (*A*-C, with *A*=B, Al, Ga, In, Tl), namely the so-called *X* centers [20–24], in silicon as benchmark systems. Group-IIIA acceptors are commonly used to create *p* type Si, whereas carbon is one of the major residual impurities in Si. The binding of the *A* and C atoms is found to be exothermic [20], so there could be a considerable amount of *A*-C complexes existing in Si, which could affect device performance (e.g., introducing noise in infrared detectors based on group-IIIA-doped Si). The *A*-C complexes are shallower than the corresponding substitutional acceptors, and the ionization energy of the former is approximately 80% of the latter [20]. The underlying mechanism of the reduction in ionization energy is not fully understood yet. Here we show that supercells containing 10^4 atoms is necessary to obtain converged ionization energies of *A*-C complexes. While the potential-patching method based on semilocal DFT calculations underestimates the ionization energies, the hybrid-functional correction significantly improves the results and yields good agreements with experiments. The origin of the reduced ionization energies of the *A*-C complexes is further explored, and the contributions from the chemical and structural effects are analyzed in detail. The results suggest that accurate simulations of shallow impurities and their complexes can be achieved through the combination of the potential-patching method and the hybrid-functional correction.

II. COMPUTATIONAL DETAILS

The calculations are performed using PWMAT [25,26], which is a GPU-based plane-wave pseudopotential code for DFT simulations. The core-valence interaction is described by Troullier-Martins norm-conserving pseudopotentials [27]. Both the local density approximation (LDA) [28] and the Heyd-Scuseria-Ernzerhof (HSE) [29,30] hybrid functional are adopted to approximate the exchange-correlation interaction. The mixing ratio of the exact exchange energy in the HSE functional is 0.25. The plane-wave energy cutoff is set to 45 Ry, and the atomic positions are relaxed with the LDA functional until the force on each atom is smaller than 0.01 eV/Å. According to our tests as shown in Fig. S1 within the Supplemental Material, further relaxation using the HSE functional results in negligible changes in the LDA-optimized structures, which is understandable given the delocalized nature of the shallow impurity states. For supercell calculations, the Brillouin zone is sampled by the Γ point. In the potential-patching method which employs a large supercell, the impurity level energy is calculated by the folded-spectrum method (FSM) [31], which allows one to compute a few desired eigenstates near a given reference energy, and the spin-orbit coupling effect is also included in the FSM calculations.

III. ACCEPTOR IONIZATION ENERGY CALCULATIONS

A. Failure of the total energy approach with small supercells

The *A*-C complexes in Si are nearest-neighbor substitutional acceptor-carbon pairs [20,23,24], which have a trigonal symmetry as shown in Fig. 1(a). These impurity complexes are shallow acceptors, whose wave functions usually have a long-range tail expanding at the nanometer scale. However, due to the cubic scaling of conventional DFT calculations, the typical supercell size in defect simulations is limited to several hundreds of atoms. This size is too small to isolate the impurity wave function of the *A*-C complex from its periodic images. In Fig. 1(b) the impurity-state charge density of a −1 charged Al-C

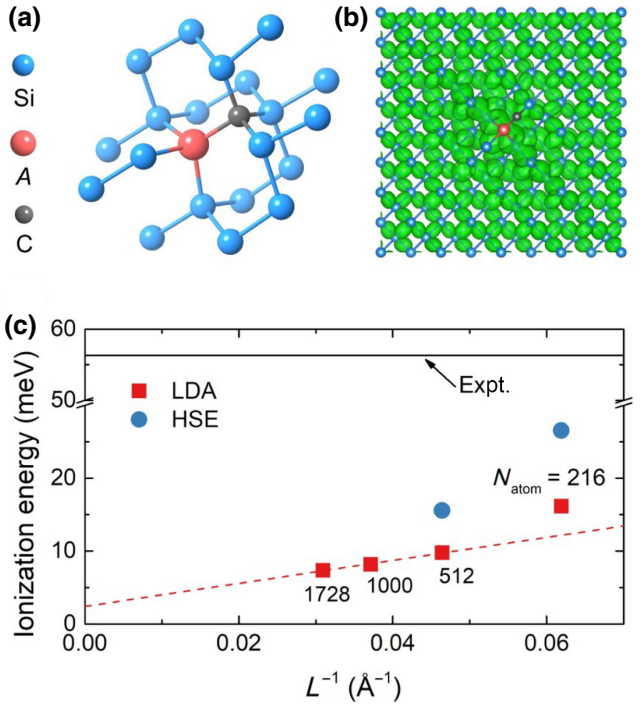

FIG. 1. (a) Structure of the A-C complexes in Si (A=B, Al, Ga, In, Tl). (b) The impurity-state charge density of a -1 charged Al-C complex in a 512-atom supercell. The isosurface contains 60% of the total charge. (c) The calculated acceptor ionization of the Al-C complex using Eq. (1) with different supercell size.

complex in a 512-atom supercell is presented, and the isosurface contains 60% of the total charge. It is seen that the charge is delocalized over the whole supercell. The artificial wave-function overlap between the periodic images can lead to qualitative errors in the calculated ionization energies.

According to the defect formation energy theory based on supercell total energy calculations, the impurity-charge transition level relative to the bulk valence-band maximum (VBM) can be calculated by [6,32]

$$\epsilon_{\rm im}(q/q') = \frac{E(\alpha,q) - E(\alpha,q') + (q-q')E_{\rm VBM}}{q'-q}, \quad (1)$$

where $E(\alpha,q)$ is the total energy of the supercell containing the impurity α at a charge state q, and $E_{\rm VBM}$ is the VBM energy of the impurity-free host material. The acceptor ionization energy of an A-C complex corresponds to the transition level $\epsilon_{\rm im}(0/-1)$ between 0 and -1 charged states. Ideally, the supercell size effect can be removed through the extrapolation to infinite supercell length L. Although this approach works well for deep impurities with localized wave functions [33–35], it could fail for shallow impurities due to the artificial interactions between supercell images introduced by the overlap of delocalized wave functions. For example, even for a neutral shallow impurity, there could be long-range Coulomb interactions between supercell images, because the overlapped impurity states act as the background charge. This leads to a nonphysical size dependence of the total energy [36,37]. To demonstrate this, we calculate the ionization energy $\epsilon_{\rm im}(0/-1)$ of an Al-C complex in cubic supercells using Eq. (1) with LDA. The supercell length L ranges from $3a$ to $6a$ (corresponding to 216 to 1728 atoms), where $a = 5.39$ Å is the LDA-optimized lattice constant of Si. The final $\epsilon_{\rm im}(0/-1)$ obtained from the extrapolation to infinite L is 2.4 meV [see Fig. 1(c)], much smaller than the experimental value of 56.3 meV [20]. One may expect that the disparity is a result of the self-interaction error of LDA, and should be recovered by HSE. However, our HSE calculations with these small supercells only slightly increase the ionization energy. As seen in Fig. 1(c), for the 512-atom supercell, the $\epsilon_{\rm im}(0/-1)$ calculated by HSE is only 5 meV larger than that by LDA. Therefore, the main source of the error should be attributed to the artificial overlap of impurity state wave functions, therefore an extremely large supercell is needed to remove this effect, which could exceed the capability of conventional DFT calculations.

B. The potential-patching method for shallow impurities

In an alternative approach, the impurity ionization energy can be evaluated by separately considering the contributions from electronic excitations and structural relaxations [38,39]. For example, for the transition between the neutral and -1 charged states of an acceptor α, Eq. (1) can be rewritten as

$$\begin{aligned}\epsilon_{\rm im}(0/-1) = {} & [E(\alpha,-1,\mathbf{R}_{-1}) - E(\alpha,0,\mathbf{R}_{-1})] \\ & + [E(\alpha,0,\mathbf{R}_{-1}) - E(\alpha,0,\mathbf{R}_0)] \\ & - E_{\rm VBM}, \end{aligned} \quad (2)$$

here $E(\alpha,q,\mathbf{R}_{q'})$ indicates the total energy of the doped supercell with a charge state q at the fully relaxed geometry $\mathbf{R}_{q'}$ of a charge state q'. For shallow impurities, because of the delocalized nature of the impurity wave function, the contribution from the structural relaxation due to the occupation change of the impurity state, namely the $E(\alpha,0,\mathbf{R}_{-1}) - E(\alpha,0,\mathbf{R}_0)$ term, is quite small. According to our calculations, for the A-C complexes in the present study, this term is only approximately 1 meV, and thus can be safely ignored. On the other hand, the electronic excitation contribution $E(\alpha,-1,\mathbf{R}_{-1}) - E(\alpha,0,\mathbf{R}_{-1})$ is the ionization potential of the doped supercell in the -1 charge state at the $\mathbf{R}_{-1}$ geometry, which corresponds to the quasiparticle energy $E_{\rm im}(-1)$ of the occupied acceptor state (it is also the highest occupied state of the doped supercell). The shallow acceptor level thus can be calculated by $\epsilon_{\rm im}(0/-1) = E_{\rm im}(-1) - E_{\rm VBM}$ [in the following, the notion $(0/-1)$ is omitted since we focus on the $\epsilon_{\rm im}(0/-$

1) level in the whole study]. Note the -1 charged impurity system is a closed-shell system with a clear band gap, ensuring fast convergence of the potential, and all of the following calculations are based on this closed-shell system. While in principle $E_{\rm im}$ and $E_{\rm VBM}$ should be computed by solving the quasiparticle equation (e.g., the *GW* method [40,41]), in the following we first consider the single-particle Kohn-Sham equation with the LDA exchange-correlation functional as an approximation of the quasiparticle equation, thus $E_{\rm im}$ and $E_{\rm VBM}$ are determined by the Kohn-Sham eigenenergies. Then we discuss the correction scheme.

To get the $E_{\rm im}$ free from supercell image interaction, it is essential to obtain the local potential $V_{\rm im}(\mathbf{r})$ at the infinite L limit. $V_{\rm im}(\mathbf{r})$ includes the ion potential, the Hartree potential, and the exchange-correlation potential. Here we adopt a potential-patching approach [8]. When the system is -1 charged, the corresponding $V_{\rm im}(\mathbf{r})$ has a long-range potential tail $1/\varepsilon r$ due to the screened Coulomb interaction, where ε is the bulk dielectric constant. At a position $\mathbf{r}$ far away from the impurity, $V_{\rm im}(\mathbf{r})$ can be well approximated as $V_{\rm im}(\mathbf{r}) = V_{\rm bulk}(\mathbf{r}) + 1/\varepsilon r$, where $V_{\rm bulk}(\mathbf{r})$ is the local potential of the perfect bulk Si. Therefore, the key point is to determine the $V_{\rm im}(\mathbf{r})$ for $\mathbf{r}$ close to the impurity. In this case $V_{\rm im}(\mathbf{r})$ can be expressed as $V_{\rm bulk}(\mathbf{r}) + \Delta V(\mathbf{r})$, in which the $\Delta V(\mathbf{r})$ term contains the contributions from the screened Coulomb potential of the -1 charge, the chemical difference between the impurity and the host, and the impurity-induced lattice distortion. The latter two contributions are short ranged, namely, $\Delta V(\mathbf{r}) - 1/\varepsilon r \to 0$ when r is large compared to the lattice constant. Due to the short-range nature of the $\Delta V(\mathbf{r}) - 1/\varepsilon r$ term, the $V_{\rm im}(\mathbf{r})$ near the impurity can be evaluated using a supercell with a moderate size. Here we construct a cubic 512-atom Si supercell containing an A-C complex (Ω_{512}), and the A atom is placed at the cell center. The supercell is -1 charged and has 2048 valence electrons. After full relaxation, structural distortion is found to mainly occur near the impurity. The atomic displacement at the cell boundary is negligible (see Fig. S1 within the Supplemental Material [42]), indicating the supercell size is sufficiently large to accommodate the atomic relaxation. After self-consistent calculations with LDA, one can obtain the local potential $V_{\rm im}^{\rm SC}(\mathbf{r})$ of the impurity supercell.

Now, the $V_{\rm im}^{\rm SC}(\mathbf{r})$ includes all the short-range effects caused by the A-C complex. However, as a result of the periodic boundary condition, it also contains the $1/\varepsilon r$ Coulomb potential tails from the periodic images of the impurity. For a supercell containing an impurity at $\mathbf{r}$=0, this image potential V_C can be expressed as

$$V_C(\mathbf{r}) = \sum_{(i,j,k)\neq(0,0,0)} \frac{1}{\varepsilon|\mathbf{r} - (i\mathbf{L}_1 + j\mathbf{L}_2 + k\mathbf{L}_3|)}, \qquad (3)$$

in which $\mathbf{L}_1$, $\mathbf{L}_2$, and $\mathbf{L}_3$ are the supercell lattice vectors. For the cubic 512-atom Si cell, $|\mathbf{L}_1| = |\mathbf{L}_2| = |\mathbf{L}_3| = 4a$. To obtain the $V_{\rm im}(\mathbf{r})$ for $\mathbf{r} \in \Omega_{512}$, the $V_C(\mathbf{r})$ should be removed from the $V_{\rm im}^{\rm SC}(\mathbf{r})$. In order to calculate the $V_C(\mathbf{r})$, one can construct a spherical model charge density $\rho_{\rm mod}(\mathbf{r})$ localized within Ω_{512}. The $V_C(\mathbf{r})$ can be then determined by the difference between the electrostatic potential of $\rho_{\rm mod}(\mathbf{r})$ under periodic boundary condition with the same 512-atom cell [$V_{\rm mod}^{\rm SC}(\mathbf{r})$] and that under open boundary condition [$V_{\rm mod}^{\rm iso}(\mathbf{r})$] [8,43,44]. As mentioned above, for $\mathbf{r}$ outside Ω_{512}, $V_{\rm im}(\mathbf{r})$ can be well approximated by the bulk potential plus the $1/\varepsilon r$ tail. Hence, the total $V_{\rm im}(\mathbf{r})$ free from the image interaction in a supercell of arbitrary size can be constructed by patching the $\mathbf{r} \in \Omega_{512}$ and $\mathbf{r} \notin \Omega_{512}$ components together:

$$V_{\rm im}(\mathbf{r}) = \begin{cases} V_{\rm im}^{\rm SC}(\mathbf{r}) - V_C(\mathbf{r}) + V_{\rm align}, & \mathbf{r} \in \Omega_{512} \\ V_{\rm bulk}(\mathbf{r}) + 1/\varepsilon r. & \mathbf{r} \notin \Omega_{512}. \end{cases} \qquad (4)$$

The $V_{\rm align}$ here is a constant potential alignment term to ensure the potentials inside and outside Ω_{512} match each other. To have a more realistic description on the $1/\varepsilon r$ Coulomb potential tail and impurity wave-function distribution, the experimental dielectric constant [45] ε=11.9 of silicon is used in our calculations. Note the experimental and LDA dielectric constants are quite close (11.9 versus 12.3), and the use of the LDA dielectric constant only leads to a 2-meV difference in the ionization energy. An illustration scheme of the potential-patching method is presented in Fig. 2.

To see whether the potential-patching method works well for the A-C complexes, we examine the generated $V_{\rm im}(\mathbf{r})$ for the Al-C complex with -1 charge based on LDA calculations. Ideally, the potential difference between the generated $V_{\rm im}(\mathbf{r})$ and $V_{\rm bulk}(\mathbf{r})$ should coincide with the $1/\varepsilon r$ tail at the cell boundary of Ω_{512}. In Fig. 3, the atomic site potential difference ΔV_i between the impurity system and bulk as a function of distance from the Al atom is plotted. ΔV_i is calculated as

$$\begin{aligned} \Delta V_i(R_{\text{Al-}i}) &= V_i^{\rm atom}({\rm im}) - V_i^{\rm atom}({\rm bulk}), \\ V_i^{\rm atom}({\rm im}) &= \int \rho_{\rm G}(\mathbf{r} - \mathbf{R}_i^{\text{Al-C}}) V_{\rm im}(\mathbf{r}) d\mathbf{r}, \\ V_i^{\rm atom}({\rm bulk}) &= \int \rho_{\rm G}(\mathbf{r} - \mathbf{R}_i^{\rm bulk}) V_{\rm bulk}(\mathbf{r}) d\mathbf{r}. \end{aligned} \qquad (5)$$

Here $\mathbf{R}_i^{\text{Al-C}}$ and $\mathbf{R}_i^{\rm bulk}$ are the equilibrium positions of atom i in the Al-C complex system and bulk, respectively, and $R_{\text{Al-}i} = |\mathbf{R}_i^{\text{Al-C}} - \mathbf{R}_{\rm Al}^{\text{Al-C}}|$ is the distance between the atom i and Al. $\rho_{\rm G}$ is a Gaussian unit charge centered at atom i. It is seen in Fig. 3 that the ΔV_i indeed follows $1/\varepsilon R_{\text{Al-}i}$, as the $\Delta V_i - 1/\varepsilon R_{\text{Al-}i}$ rapidly decreases to 0 when $R_{\text{Al-}i}$ is larger than approximately 8 Å. Hence, the generated

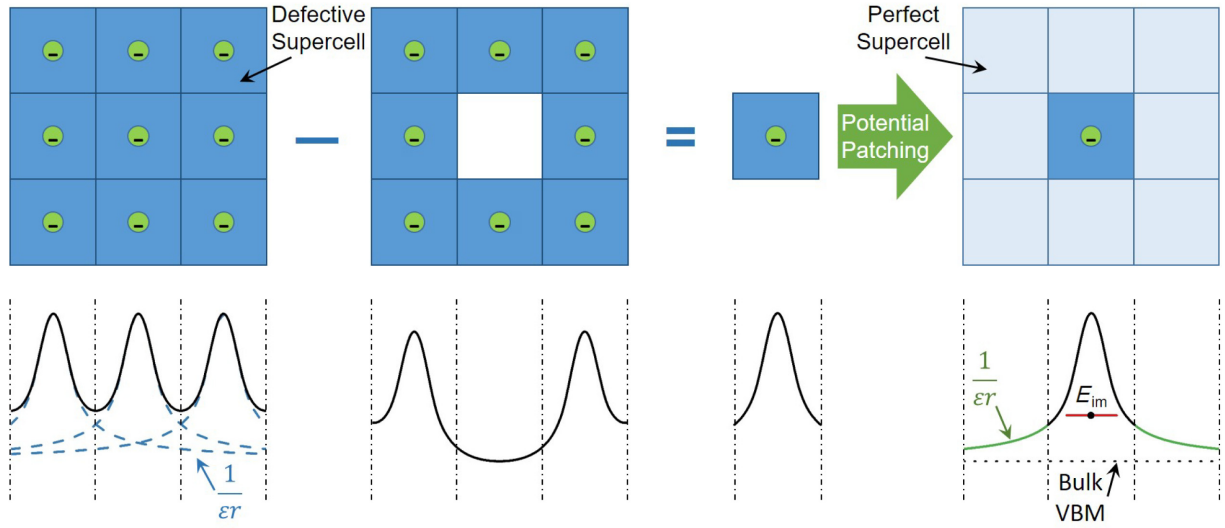

FIG. 2. Illustration scheme of the potential-patching method.

$V_{\rm im}(\mathbf{r})$ well describes the local potential of an isolated Al-C complex. We also analyze the potential discontinuity at the cell boundary of Ω_{512} and find the grid-averaged absolute value of the potential mismatch is only approximately 10 meV. Such a small discontinuity ensures the applicability of the potential-patching method, and should not cause any significant effects in the final results. For comparison, we also calculate the atomic site potential difference $\Delta V_i^{\rm SC}$ between $V_{\rm im}^{\rm SC}(\mathbf{r})$ and $V_{\rm bulk}(\mathbf{r})$. As expected, $\Delta V_i^{\rm SC}(R_{\text{Al-}i})$ does not exhibit the $1/\varepsilon R_{\text{Al-}i}$ behavior due to the supercell image interaction. Therefore, we conclude that the potential-patching method can successfully remove the Coulomb potential tail from the periodic images for the -1 charged A-C complexes.

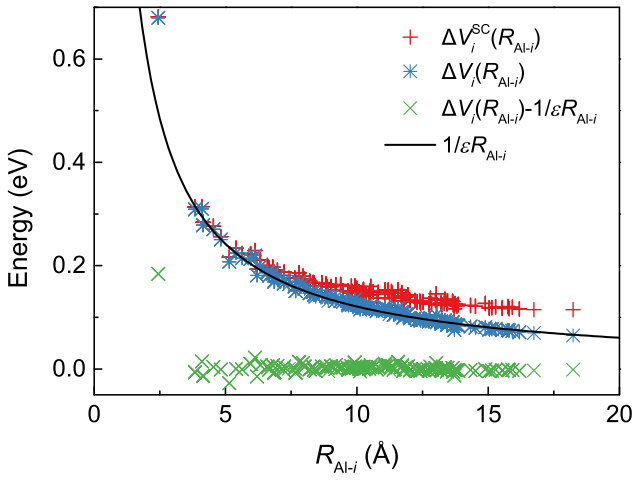

FIG. 3. Atomic-site potentials for a 512-atom supercell containing an Al-C complex as a function of distance from the Al atom. The results before and after the removal of the image Coulomb interaction are both presented.

Once we obtain the $V_{\rm im}(\mathbf{r})$ with LDA, the eigenenergy $E_{\rm im}$ of the impurity state can be calculated by solving the Kohn-Sham equation:

$$\left(-\frac{1}{2}\nabla^2 + V_{\rm im}(\mathbf{r}) + \hat{V}_{\rm NL}\right)\psi_{\rm im}(\mathbf{r}) = E_{\rm im}\psi_{\rm im}(\mathbf{r}), \qquad (6)$$

where $\hat{V}_{\rm NL}$ is the nonlocal pseudopotential. Note in the potential-patching approach, the alignment term $V_{\rm align}$ ensures that $V_{\rm im}(\mathbf{r})$ and $V_{\rm bulk}(\mathbf{r})$ have the same energy reference. Therefore, one can directly compare $E_{\rm im}$ and $E_{\rm VBM}$, and get the acceptor ionization energy $\epsilon_{\rm im} = E_{\rm im} - E_{\rm VBM}$. To calculate the ionization energies for the A-C complexes, we construct cubic supercells with sizes ranging from $8a$ to $20a$ to generate the $V_{\rm im}(\mathbf{r})$, using the same central cell size of 512 atom as in Eq. (4). The corresponding numbers of atoms in the supercells are from 4096 to 64 000. The different supercell sizes allow us to obtain converged $\epsilon_{\rm im}$ through extrapolation, and to explore size effects. For these large supercells, the corresponding Kohn-Sham equations are solved using the FSM [31], which allows one to compute a few desired eigenstates near a given reference energy, and the spin-orbit coupling effect is also included.

The calculated acceptor ionization energies $\epsilon_{\rm im}^{\rm LDA}$ of the A-C complexes in Si, with the LDA exchange-correlation functional, are listed in Table I. The results are extrapolated to infinite supercell length using an exponential decay function to obtain converged values $[\epsilon_{\rm im}^{\rm LDA}(\infty)]$. It is seen that the calculated $\epsilon_{\rm im}^{\rm LDA}$ decreases as the supercell size increases, which can be attributed to the reduced confinement of the impurity wave function. In general, the $\epsilon_{\rm im}^{\rm LDA}$ obtained with the 4096-atom supercell are significantly larger than the $\epsilon_{\rm im}^{\rm LDA}(\infty)$, indicating that the impurity wave function can spread over thousands of atoms, thus larger supercells with approximately 10^4 atoms are necessary for

TABLE I. The LDA calculated acceptor ionization energies $\epsilon_{\rm im}^{\rm LDA}$ of the A-C complexes in Si with the potential-patching method using different supercell lengths L. The results are extrapolated to infinite supercell length using an exponential decay function to obtain converged values. Experimental results [20] are also given. The unit is meV.

	$\epsilon_{\rm im}^{\rm LDA}$				
Cell length	B-C	Al-C	Ga-C	In-C	Tl-C
$L = 8a$	71.64	75.44	75.04	84.45	105.33
$L = 12a$	51.39	54.84	54.43	65.29	92.38
$L = 16a$	42.39	46.43	45.93	59.38	90.02
$L = 20a$	38.30	43.12	42.52	57.76	89.60
$L \to \infty$	35.04	40.80	40.10	56.95	89.50
Expt. [20]	37.1	56.3	57.0	112.8	180

shallow impurity calculations. For instance, for the shallowest B-C complex, a 64 000-atom supercell is needed to ensure a reasonable convergence. In Table I, the experimental acceptor ionization energies are also presented. The calculated $\epsilon_{\rm im}^{\rm LDA}$ reproduces the trend in experiments, i.e., it increases when the A atom goes from B to Tl. However, compared to experimental results, there is an overall underestimation in the calculated $\epsilon_{\rm im}^{\rm LDA}$. The underestimation is larger for a deeper impurity, increasing from approximately 2 meV for B-C to approximately 90 meV for Tl-C. Since the structural relaxation contribution $E(\alpha, 0, \mathbf{R}_{-1}) - E(\alpha, 0, \mathbf{R}_0)$ is negligible, the source of the error should come from the fact that the $E_{\rm im}$ and $E_{\rm VBM}$ determined by the Kohn-Sham eigenvalues are not true quasiparticle energies, because the LDA Kohn-Sham equation cannot well approximate the exact quasiparticle equation for this problem, partly due to the self-interaction error. To obtain more accurate acceptor ionization energies, a correction scheme is needed to remove the LDA error.

C. A hybrid-functional correction

In the GW approach, the first-order correction to the LDA eigenenergy $E_j^{\rm LDA}$ to calculate the quasiparticle energy $E_j^{\rm QP}$ for a state j is [46]

$$\begin{aligned}\Delta E_j^{\rm QP} &= E_j^{\rm QP} - E_j^{\rm LDA} \\ &= \langle \psi_j^{\rm LDA} | \Sigma(E_j^{\rm QP}) - V_{\rm xc}^{\rm LDA} | \psi_j^{\rm LDA} \rangle. \end{aligned} \tag{7}$$

Here $\psi_j^{\rm LDA}$ is the LDA wave function, $V_{\rm xc}^{\rm LDA}$ is the exchange-correlation potential, and Σ is the nonlocal self-energy. Therefore, the quasiparticle correction to the LDA calculated ionization energy should be $\Delta\epsilon_{\rm im}^{\rm QP} = \Delta E_{\rm im}^{\rm QP} - \Delta E_{\rm VBM}^{\rm QP}$, namely, the difference between the quasiparticle energy corrections for the impurity state and the bulk VBM. Because the -1 charged A-C complex systems and bulk Si are all closed-shell systems with a clear band gap, their GW self-energies Σ are short ranged [47,48]. As a result, the self-energy effects can be effectively represented by modifications to the nonlocal pseudopotentials using some spherical and short-ranged functions $V_{\rm ps}(r)$ that reproduces the $\Delta E_j^{\rm QP}$ [49–51]. For the ionization energy calculations, what matters is the difference between $\Delta E_{\rm im}^{\rm QP}$ and $\Delta E_{\rm VBM}^{\rm QP}$, which is mainly determined by the difference between the self-energy operators of the impurity system ($\Sigma_{\rm im}$) and bulk Si ($\Sigma_{\rm bulk}$). One can expect that the $\Sigma_{\rm im}$ and $\Sigma_{\rm bulk}$ only significantly differ at the vicinity of the impurity site, thus the difference can be well described using a relatively small supercell, and the correction terms $V_{\rm ps}(r)$ can be applied only to the impurity and/or its nearby atoms, with the requirement that the energy shift $\Delta\epsilon_{\rm im}^{\rm QP} = \Delta E_{\rm im}^{\rm QP} - \Delta E_{\rm VBM}^{\rm QP}$ for the impurity state in this small supercell is well reproduced. Then one can use the same $V_{\rm ps}(r)$ in a much larger supercell to remove the error cause by the LDA potential.

To determine the $V_{\rm ps}(r)$, in principle the $\Delta E_{\rm im}^{\rm QP}$ and $\Delta E_{\rm VBM}^{\rm QP}$ should be computed with the GW method. Because of the high computational costs, in practice the applications of the GW method is often limited to supercells with several tens of atoms or less. However, a sufficiently large supercell that accommodates the full relaxation of atoms is crucial for determining $V_{\rm ps}(r)$. While a 64-atom supercell works for single-atom-doped Si [18], the A-C complexes studied here requires a larger supercell. As mentioned, the 512-atom supercell is able to encompass all the atomic relaxation, but it is difficult to perform a GW calculation for such a large supercell. Here, we propose to perform HSE hybrid-functional calculations instead of the GW method to determine the $V_{\rm ps}(r)$. More specifically, we require

$$E_{\rm im}^{\rm HSE}(\Omega_{512}) - E_{\rm VBM}^{\rm HSE} = E_{\rm im}^{\rm LDA+C}(\Omega_{512}) - E_{\rm VBM}^{\rm LDA}, \tag{8}$$

where $E_{\rm im}^{\rm HSE}(\Omega_{512})$ and $E_{\rm im}^{\rm LDA+C}(\Omega_{512})$ are the impurity eigenenergies in Ω_{512} calculated by the HSE functional and the LDA potential plus the $V_{\rm ps}(r)$ correction, respectively. $E_{\rm VBM}^{\rm HSE}$ and $E_{\rm VBM}^{\rm LDA}$ are bulk VBM from HSE and LDA, respectively. We expect that replacing GW by HSE would work reasonably well. By mixing a portion of exact exchange energy to the exchange-correlation functional, the HSE functional restores, to a large extent, the linearity of the total energy with respect to the occupation [52]. Hence, it satisfies the generalized Koopmans' condition [19] fairly well, and the HSE eigenenergies could be a reasonable approximation to the quasiparticle energies, especially for simple s-p bonded semiconductors like Si [53]. Moreover, many studies have demonstrated that the overall accuracy of the defect and impurity levels predicted by HSE is comparable to that of GW calculations [54,55].

Because the impurity state of the A-C complex is mainly contributed by the atomic p orbitals, we apply the correction $V_{\rm ps}(r) = \beta \sin(\pi r/r_c)/r$ for $r < r_c$ to the p nonlocal pseudopotential of the A atom. For $r > r_c$, the $V_{\rm ps}(r)$ is

TABLE II. The HSE-corrected acceptor ionization energies $\epsilon_{\rm im}^{\rm LDA+C}$ of A-C complexes calculated with different supercell size L. The unit is meV.

	$\epsilon_{\rm im}^{\rm LDA+C}$				
Cell length	B-C	Al-C	Ga-C	In-C	Tl-C
$L = 8a$	75.95	83.75	83.53	115.05	171.59
$L = 12a$	55.24	64.24	63.84	104.02	166.86
$L = 16a$	46.85	58.03	57.49	102.28	166.44
$L = 20a$	43.58	56.27	55.66	102.01	166.40
$L \to \infty$	41.32	55.36	54.70	101.96	166.40
Expt. [20]	37.1	56.3	57.0	112.8	180

0. β and r_c are adjusting parameters. We first perform LDA and HSE self-consistent calculations for a 512-atom supercell with a -1 charged A-C complex to obtain $E_{\rm im}^{\rm HSE}(\Omega_{512})$ and $E_{\rm im}^{\rm LDA}(\Omega_{512})$, and for a bulk cell to obtain $E_{\rm VBM}^{\rm HSE}$ and $E_{\rm VBM}^{\rm LDA}$. Next, we apply $V_{\rm ps}(r)$ to the p orbital of the A atom, and perform a non-self-consistent calculation for the impurity 512-atom supercell using the LDA local potential $V_{\rm im}^{\rm SC}(\mathbf{r})$ from the previous self-consistent calculation. Note that non-self-consistent calculations are adopted here instead of self-consistent calculations, mimicking the G_0W_0 approach where the total charge density is not updated. With non-self-consistent calculations, there is no modification on the total charge density induced by $V_{\rm ps}(r)$, and a $V_{\rm ps}(r)$ with a relatively small magnitude can be used. The β and r_c are tuned, so that the impurity state eigenenergy $E_{\rm im}^{\rm LDA+C}(\Omega_{512})$ satisfies Eq. (8), namely, compared to the case without the pseudopotential modification, it is shifted by the difference in the HSE and LDA ionization energies of Ω_{512}. The fitted β and r_c are given in Table S1 within the Supplemental Material [42]. Then, based on $V_{\rm im}^{\rm SC}(\mathbf{r})$, we use the potential-patching method as described above to generate the $V_{\rm im}(\mathbf{r})$ in a large supercell. The corrected impurity eigenenergy $E_{\rm im}^{\rm LDA+C}$ is computed with the $V_{\rm im}(\mathbf{r})$ and the $V_{\rm ps}$-modified pseudopotential of the A atom. Finally, the acceptor level $\epsilon_{\rm im}^{\rm LDA+C}$ is determined by the difference between $E_{\rm im}^{\rm LDA+C}$ and the bulk VBM $E_{\rm VBM}^{\rm LDA}$. The results are listed in Table II. It is seen that the HSE correction results in larger acceptor ionization energies compared to LDA, and the calculated ionization energies agree with experiments quite well. For B-C, Al-C, and Ga-C, the errors are just a few meVs. For deeper In-C and Tl-C levels, the errors are 11 and 14 meV, respectively, which remain small compared to the magnitude of their level depth (0.1–0.2 eV). Note LDA underestimates the lattice constant of Si by 1%, which might be one of the sources of the slight disagreements with experiments. The good agreements between the calculated and experimental results suggest that the combination of the potential patching method and the HSE correction scheme is a promising approach for accurate calculations of shallow impurity levels.

IV. THE IMPURITY STATES OF A-C COMPLEXES

A. Wave-function characters

With the potential-patching method and the HSE correction, not only the impurity levels, but also the impurity wave functions of the A-C complexes can be calculated. The wave-function overlap between periodic images can be avoided using the 64 000-atom supercell, allowing one to analyze the character of the impurity state. With spin-orbit coupling, the calculated impurity states of the A-C complexes are twofold degenerated, consistent with experiments [24]. In Fig. 4(a), the spherical averages of the impurity wave-function square versus the distance to the A atom in the 64 000-atom supercell are shown for all the A-C complexes. The exponential decay behavior of the wave functions is clearly observed. The wave-function tail can be approximated by an envelope function $F(r) = F_0 \exp(-r/a_{\rm Bohr}^*)$, where F_0 is a constant, and $a_{\rm Bohr}^*$ is the effective Bohr radius, which qualitatively describes the extent of the impurity wave-function localization. The wave-function square thus follows $|F(r)|^2$. The fitted $a_{\rm Bohr}^*$ for the A-C complexes are given in the inset of Fig. 4(a). The $a_{\rm Bohr}^*$ decreases as the acceptor level become deeper from B-C to Tl-C. For B-C, Al-C, and Ga-C, their $a_{\rm bohr}^*$ are larger than 10 Å, indicating a strong character of wave-function delocalization. In Fig. 4(b), the charge density of the impurity state of the Al-C complex is presented. The isosurface contains 80% of the total charge. The C_{3v} symmetry of the Al-C complex results in strong anisotropy in the wave function. The impurity state is more extended within the Si (111) plane than along the [111] direction. The strong anisotropy suggests a significant central-cell correction effect, which is missing in the hydrogen model

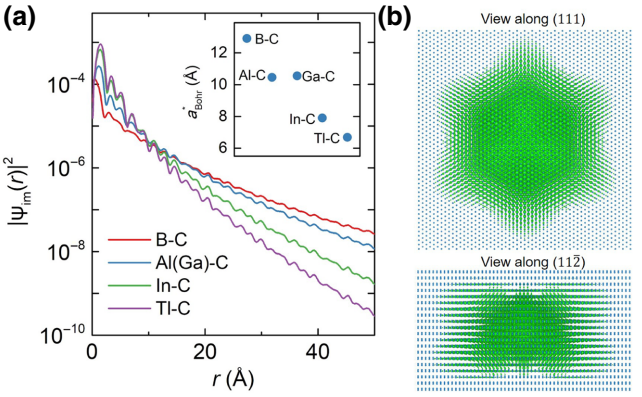

FIG. 4. (a) Spherical averages of the wave-function square of the A-C complexes versus the distance to the A atom in the 64 000-atom supercell. The results for Al-C and Ga-C are almost identical. The fitted effective Bohr radius are also given in the inset. (b) The charge density of the impurity state of the Al-C complex in the 64 000-atom supercell. The isosurface contains 80% of the total charge.

under the effective mass theory. By probing the wavefunction distribution around the Al-C complex (Fig. S2 within the Supplemental Material [42]), it is found that the p orbitals of the Al atom and the C atom have opposite phases and there is a nodal surface between them, indicating a p-p π^* antibonding interaction, in agreement with a previous study [56].

B. Origin of ionization energy reduction

Experimentally, it is found that, compared to the single substitutional group-IIIA acceptors in Si ($A_{\rm Si}$), the formation of the A-C complexes results in an approximately 20% reduction in the ionization energy [20]. However, the mechanism of the ionization energy reduction is not fully understood yet. In this part, we explore the origin of this reduction. Here, we use our potential-patching method with the HSE correction to compute the ionization energy of the $A_{\rm Si}$ (the details of the pseudopotential correction used is given in Table S2 within the Supplemental Material [42]), and the results are listed in Table III. It is seen that our procedure yields good agreements with experiments [20] and previous GW-based calculations [18]. The calculated acceptor ionization energy change $\Delta\epsilon_{\rm im}^{\rm diff}$ of the A-C complexes with respect to the $A_{\rm Si}$ is shown in Fig. 5(a) (a negative value indicates a reduction in ionization energy). The magnitude of $\Delta\epsilon_{\rm im}^{\rm diff}$ are consistent with experiments.

In general, there could be two factors that contribute to the reduction of ionization energy [57]. The first one is the chemical interaction (CI) between the A atom and the C atom. The second one is the strain-field effect, namely the global structural distortion (SD) of the Si lattice due to the incorporation of the C atom. Correspondingly, we can decompose the formation of the A-C complexes into two processes CI and SD. This is done by constructing an intermediate configuration ($\mathbf{R}_{\rm inter}$) between fully relaxed structures of the single-A dopant ($\mathbf{R}_A$) and the A-C complex ($\mathbf{R}_{A\text{-C}}$). Starting from $\mathbf{R}_A$, we replace a neighboring Si atom of the A atom by a C atom, and then the $\mathbf{R}_{\rm inter}$ is generated by only relaxing the A and the C atoms as well as their nearest-neighboring Si atoms (eight atoms are relaxed in total). All the other Si atoms are kept at their positions in $\mathbf{R}_A$. The acceptor ionization energy in the intermediate configuration are calculated using the potential-patching method, with the same HSE corrections as for the fully relaxed A-C complexes. As a result, the CI process $\mathbf{R}_A \rightarrow \mathbf{R}_{\rm inter}$ contains all the chemical effects, and the SD process $\mathbf{R}_{\rm inter} \rightarrow \mathbf{R}_{A\text{-C}}$ includes the structural effects. Then we have

$$\begin{aligned}\Delta\epsilon_{\rm im}({\rm CI}) &= \epsilon_{\rm im}(\mathbf{R}_{\rm inter}) - \epsilon_{\rm im}(\mathbf{R}_A),\\ \Delta\epsilon_{\rm im}({\rm SD}) &= \epsilon_{\rm im}(\mathbf{R}_{A\text{-C}}) - \epsilon_{\rm im}(\mathbf{R}_{\rm inter}),\\ \Delta\epsilon_{\rm im}^{\rm diff} &= \epsilon_{\rm im}(\mathbf{R}_{A\text{-C}}) - \epsilon_{\rm im}(\mathbf{R}_A)\\ &= \Delta\epsilon_{\rm im}({\rm CI}) + \Delta\epsilon_{\rm im}({\rm SD}).\end{aligned} \tag{9}$$

Here $\Delta\epsilon_{\rm im}({\rm CI})$ and $\Delta\epsilon_{\rm im}({\rm SD})$ are the contributions of the CI and SD processes to the ionization energy reduction. $\epsilon_{\rm im}(\mathbf{R}_A)$, $\epsilon_{\rm im}(\mathbf{R}_{\rm inter})$, and $\epsilon_{\rm im}(\mathbf{R}_{A\text{-C}})$ are the calculated ionization energies of the $A_{\rm Si}$, the intermediate structure, and the A-C complex.

In Fig. 5(b), the calculated $\Delta\epsilon_{\rm im}({\rm CI})$ and $\Delta\epsilon_{\rm im}({\rm SD})$ are presented. For A=B, Al, and Ga, the $\Delta\epsilon_{\rm im}({\rm CI})$ is slightly positive, therefore it tends to increase the ionization energy. However, the negative SD contribution dominates over the CI contribution, leading to the overall reduction in the ionization energy. For A=In and Tl, the situation is different. Both the $\Delta\epsilon_{\rm im}({\rm CI})$ and $\Delta\epsilon_{\rm im}({\rm SD})$ are negative and have similar magnitudes, indicating that the ionization energy reduction in these systems is a joint effect of CI and SD. It is interesting to note that the CI has opposite effects for the two groups of dopants, which can be understood by a competition mechanism. For the impurity state, there are two types of chemical interaction between the A and C atoms. One is the p-p π^* antibonding interaction as mentioned above, which tends to push up the impurity level and increase the ionization energy. The other type of interaction is the charge transfer between A and C atoms. Compared to the case of $A_{\rm Si}$, there will be an

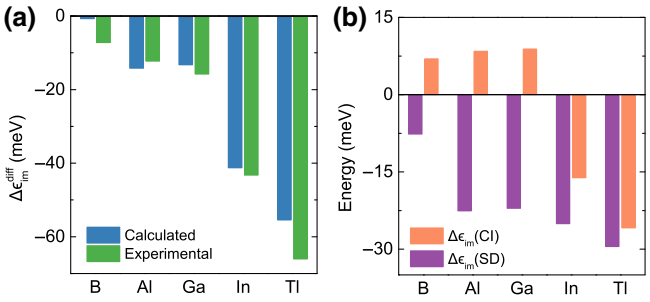

FIG. 5. (a) Calculated and experimental acceptor ionization energy change $\Delta\epsilon_{\rm im}^{\rm diff}$ of the A-C complexes with respect to the $A_{\rm Si}$. (b) The CI and SD contributions to the $\Delta\epsilon_{\rm im}^{\rm diff}$.

TABLE III. Acceptor ionization energies $\epsilon_{\rm im}^{\rm LDA+C}$ of $A_{\rm Si}$ calculated by the potential patching method with the HSE correction using different supercell lengths L. Experimental results [20] and theoretical values from GW-based calculations [18] are also listed for comparison. The unit is meV.

	$\epsilon_{\rm im}^{\rm LDA+C}$				
Cell length	B	Al	Ga	In	Tl
$L = 8a$	76.92	94.10	93.36	152.18	225.71
$L = 12a$	55.89	75.72	74.51	144.16	222.04
$L = 16a$	47.46	71.00	69.55	143.27	221.81
$L = 20a$	44.22	69.93	68.39	143.18	221.78
$L \rightarrow \infty$	42.02	69.50	67.91	143.16	221.78
GW-based Calc. [18]	44	62	71	139	246
Expt. [20]	44.3	68.5	72.7	156.0	246.0

additional charge transfer from the A atom to the C atom in the A-C complex, since C has a larger electronegativity than Si. As a result, the charge transfer decreases the electrostatic potential around the A site, lowers the impurity level, and tends to reduce the ionization energy. Whether the CI increase or decrease the ionization energy depends on the competition between the antibonding interaction and the charge transfer effect. According to our calculations, the relaxed A-C bond lengths increase from 1.76 to 2.37 Å when A goes from B to Tl, therefore the A-C antibonding interaction becomes weaker from B to Tl. On the other hand, the additional charge transfer from the A atom due to the incorporation of C is around 0.1 e for all A-C complexes. Therefore, for the cases of B, Al, and Ga, the positive CI contribution can be attributed to the stronger A-C antibonding, which dominates over the charge transfer effect. For In and Tl, it is the charge transfer effect that dominates due to the weaker antibonding interaction, hence the CI contribution is negative.

The understanding on the interplay between antibonding, charge transfer, and structural relaxation effects brings valuable insights for experimental dopant engineering on the key factors that affects the ionization energy of shallow impurities. These discoveries further demonstrate the capability of the potential-patching method to qualitatively describe the shallow impurities at the atomic scale, as it can provide not only accurate ionization energies, but also electronic and structural details in a first-principles manner. With the fast developments in semiconductor technology, various applications of emerging semiconductor materials, such as solar cells [58,59], photocatalysts [60], photodetector [61], and field-effect transistors [62,63] are realized experimentally, where shallow dopants play important roles. However, empirical parameters are often not easy to acquire for these systems, and the potential-patching method presented here thus could be of particular interest. Moreover, besides the single crystal studied here, further developments of the current method can be extended to device-relevant structures like heterojunctions, superlattices, alloys, and nanostructures, and the shallow-level ionization energy change in these structures due to quantum confinement effect will be very interesting, and critical to the doping design in such applications.

V. CONCLUSIONS

In summary, the shallow acceptor levels of the A-C complexes in Si are studied using a potential-patching method combined with a hybrid-functional correction. The potential-patching method removes the artificial interaction between periodic images and allows the calculations of large supercells containing over 10^4 atoms to obtain converged acceptor ionization energies and wave functions. The LDA calculated acceptor ionization energies are underestimated compared with experiments, due to the failure of Kohn-Sham eigenenergies to approximate quasiparticle energies. However, it is difficult to perform quasiparticle GW calculations for a large doped supercell. To overcome this problem, based on HSE hybrid-functional calculations, which are more computationally efficient than GW, we introduce a correction potential on top of the LDA-calculated potential to mimic the quasiparticle self-energy. After the correction, the resulting acceptor ionization energies are in good agreements with experiments. The impurity wave functions of the A-C complexes could spread over thousands of atoms, and exhibit a highly anisotropic character. The origin of the acceptor ionization energy reduction of the A-C complexes compared to the single-A dopants is also analyzed. It is found that for B, Al, and Ga, the energy reduction is dominant by the structural distortion of the Si lattice due to the incorporation of the C atom. For In and Tl, the reduction is a joint effect of the structural distortion and the chemical interaction between the A and the C atoms. Our results indicate that the combination of the potential-patching method and the hybrid-functional correction could be a feasible approach for accurate simulations of shallow impurity states, and can provide theoretical insights to help experimental dopant engineering, especially when emerging semiconductors and dopants become experimentally available but empirical parameters are lacking.

ACKNOWLEDGMENTS

This work is supported by NSFC (Grants No. 12074029, No. 11991060, No. 12088101, and No. U1930402) and the Key Research Program of the Chinese Academy of Sciences (Grant No. ZDBS-SSW-WHC002). Computational resources are provided by the high-performance computing facilities at CSRC.

[1] J. M. Johnson, Z. Chen, J. B. Varley, C. M. Jackson, E. Farzana, Z. Zhang, A. R. Arehart, H.-L. Huang, A. Genc, S. A. Ringel, C. G. Van de Walle, D. A. Muller, and J. Hwang, Unusual Formation of Point-Defect Complexes in the Ultrawide-Band-Gap Semiconductor β-Ga_2O_3, Phys. Rev. X **9**, 041027 (2019).

[2] D. O. Demchenko, I. C. Diallo, and M. A. Reshchikov, Yellow Luminescence of Gallium Nitride Generated by Carbon Defect Complexes, Phys. Rev. Lett. **110**, 087404 (2013).

[3] S. Chen, J.-H. Yang, X. G. Gong, A. Walsh, and S.-H. Wei, Intrinsic point defects and complexes in the quaternary kesterite semiconductor Cu_2ZnSnS_4, Phys. Rev. B **81**, 245204 (2010).

[4] T. Mattila and R. M. Nieminen, Point-defect complexes and broadband luminescence in GaN and AlN, Phys. Rev. B **55**, 9571 (1997).

[5] K. F. Tse, S. Wang, M. H. Wong, and J. Zhu, Defects properties and vacancy diffusion in Cu_2MgSnS_4, J. Semicond. **43**, 022101 (2022).

[6] S.-H. Wei, Overcoming the doping bottleneck in semiconductors, Comput. Mater. Sci. **30**, 337 (2004).

[7] C. Freysoldt, B. Grabowski, T. Hickel, J. Neugebauer, G. Kresse, A. Janotti, and C. G. Van de Walle, First-principles calculations for point defects in solids, Rev. Mod. Phys. **86**, 253 (2014).

[8] L.-W. Wang, Density functional calculations of shallow acceptor levels in Si, J. Appl. Phys. **105**, 123712 (2009).

[9] A. Baldereschi and N. O. Lipari, Spherical model of shallow acceptor states in semiconductors, Phys. Rev. B **8**, 2697 (1973).

[10] J. C. Phillips, Dielectric theory of impurity binding energies. I. Group-V donors in Si and Ge, Phys. Rev. B **1**, 1540 (1970).

[11] J. C. Phillips, Dielectric theory of impurity binding energies. II. Donor and isoelectronic impurities in GaP, Phys. Rev. B **1**, 1545 (1970).

[12] H. Overhof and U. Gerstmann, Ab Initio Calculation of Hyperfine and Superhyperfine Interactions for Shallow Donors in Semiconductors, Phys. Rev. Lett. **92**, 087602 (2004).

[13] H. Huebl, A. R. Stegner, M. Stutzmann, M. S. Brandt, G. Vogg, F. Bensch, E. Rauls, and U. Gerstmann, Phosphorus Donors in Highly Strained Silicon, Phys. Rev. Lett. **97**, 166402 (2006).

[14] T. Yamamoto, T. Uda, T. Yamasaki, and T. Ohno, First-principles supercell calculations for simulating a shallow donor state in Si, Phys. Lett. A **373**, 3989 (2009).

[15] J. S. Smith, A. Budi, M. C. Per, N. Vogt, D. W. Drumm, L. C. L. Hollenberg, J. H. Cole, and S. P. Russo, Ab initio calculation of energy levels for phosphorus donors in silicon, Sci. Rep. **7**, 6010 (2017).

[16] M. W. Swift, H. Peelaers, S. Mu, J. J. L. Morton, and C. G. Van de Walle, First-principles calculations of hyperfine interaction, binding energy, and quadrupole coupling for shallow donors in silicon, Npj Comput. Mater. **6**, 181 (2020).

[17] H. Ma, Y.-L. Hsueh, S. Monir, Y. Jiang, and R. Rahman, Ab-initio calculations of shallow dopant qubits in silicon from pseudopotential and all-electron mixed approach, Commun. Phys. **5**, 165 (2022).

[18] G. Zhang, A. Canning, N. Grønbech-Jensen, S. Derenzo, and L.-W. Wang, Shallow Impurity Level Calculations in Semiconductors using Ab Initio Methods, Phys. Rev. Lett. **110**, 166404 (2013).

[19] S. Lany and A. Zunger, Polaronic hole localization and multiple hole binding of acceptors in oxide wide-gap semiconductors, Phys. Rev. B **80**, 085202 (2009).

[20] C. E. Jones, D. Schafer, W. Scott, and R. J. Hager, Carbon-acceptor pair centers (X centers) in silicon, J. Appl. Phys. **52**, 5148 (1981).

[21] R. Baron, M. H. Young, J. K. Neeland, and O. J. Marsh, A new acceptor level in indium-doped silicon, Appl. Phys. Lett. **30**, 594 (1977).

[22] C. Searle, M. Ohmer, and P. Hemenger, X-acceptors in silicon, Solid State Commun. **44**, 1597 (1982).

[23] F. d'Acapito, Y. Shimizu, S. Scalese, M. Italia, P. Alippi, and S. Grasso, Experimental determination of the local geometry around In and In-C complexes in Si, Appl. Phys. Lett. **88**, 212102 (2006).

[24] H. R. Chandrasekhar and A. K. Ramdas, Site symmetry and deformation-potential constants of Al-X acceptors in silicon, Phys. Rev. B **33**, 1067 (1986).

[25] W. Jia, Z. Cao, L. Wang, J. Fu, X. Chi, W. Gao, and L.-W. Wang, The analysis of a plane wave pseudopotential density functional theory code on a GPU machine, Comput. Phys. Commun. **184**, 9 (2013).

[26] W. Jia, J. Fu, Z. Cao, L. Wang, X. Chi, W. Gao, and L.-W. Wang, Fast plane wave density functional theory molecular dynamics calculations on multi-GPU machines, J. Comput. Phys. **251**, 102 (2013).

[27] N. Troullier and J. Martins, A straightforward method for generating soft transferable pseudopotentials, Solid State Commun. **74**, 613 (1990).

[28] D. M. Ceperley and B. J. Alder, Ground State of the Electron Gas by a Stochastic Method, Phys. Rev. Lett. **45**, 566 (1980).

[29] J. Heyd, G. E. Scuseria, and M. Ernzerhof, Hybrid functionals based on a screened Coulomb potential, J. Chem. Phys. **118**, 8207 (2003).

[30] A. V. Krukau, O. A. Vydrov, A. F. Izmaylov, and G. E. Scuseria, Influence of the exchange screening parameter on the performance of screened hybrid functionals, J. Chem. Phys. **125**, 224106 (2006).

[31] L.-W. Wang and A. Zunger, Solving Schrodinger's equation around a desired energy: Application to silicon quantum dots, J. Chem. Phys. **100**, 2394 (1994).

[32] S.-H. Wei and S. B. Zhang, Chemical trends of defect formation and doping limit in II-VI semiconductors: The case of CdTe, Phys. Rev. B **66**, 155211 (2002).

[33] Y. Kumagai and F. Oba, Electrostatics-based finite-size corrections for first-principles point defect calculations, Phys. Rev. B **89**, 195205 (2014).

[34] S. Lany and A. Zunger, Accurate prediction of defect properties in density functional supercell calculations, Modelling Simul. Mater. Sci. Eng. **17**, 084002 (2009).

[35] Z.-J. Suo, J.-W. Luo, S.-S. Li, and L.-W. Wang, Image charge interaction correction in charged-defect calculations, Phys. Rev. B **102**, 174110 (2020).

[36] F. Oba, A. Togo, I. Tanaka, J. Paier, and G. Kresse, Defect energetics in ZnO: A hybrid Hartree-Fock density functional study, Phys. Rev. B **77**, 245202 (2008).

[37] Y. Kumagai, M. Choi, Y. Nose, and F. Oba, First-principles study of point defects in chalcopyrite $ZnSnP_2$, Phys. Rev. B **90**, 125202 (2014).

[38] P. Rinke, A. Janotti, M. Scheffler, and C. G. Van de Walle, Defect Formation Energies without the Band-Gap Problem: Combining Density-Functional Theory and the *GW* Approach for the Silicon Self-Interstitial, Phys. Rev. Lett. **102**, 026402 (2009).

[39] W. Chen and A. Pasquarello, First-principles determination of defect energy levels through hybrid density functionals and GW, J. Phys.: Condens. Matter **27**, 133202 (2015).

[40] G. Onida, L. Reining, and A. Rubio, Electronic excitations: density-functional versus many-body Green's-function approaches, Rev. Mod. Phys. **74**, 601 (2002).

[41] F. Aryasetiawan and O. Gunnarsson, The GW method, Rep. Prog. Phys. **61**, 237 (1998).

[42] See Supplemental Material at http://link.aps.org/supplemental/10.1103/PhysRevApplied.18.064001 for the atomic relaxation in the supercell containing an Al-C complex, the wave function of the Al-C impurity state, and the details of the pseudopotential correction.

[43] C. Freysoldt, J. Neugebauer, and C. G. Van de Walle, Fully Ab Initio Finite-Size Corrections for Charged-Defect Supercell Calculations, Phys. Rev. Lett. **102**, 016402 (2009).

[44] H.-P. Komsa and A. Pasquarello, Finite-Size Supercell Correction for Charged Defects at Surfaces and Interfaces, Phys. Rev. Lett. **110**, 095505 (2013).

[45] K. V. Rao and A. Smakula, Dielectric anomalies in silicon single crystals, J. Appl. Phys. **37**, 2840 (1966).

[46] M. Shishkin and G. Kresse, Implementation and performance of the frequency-dependent GW method within the PAW framework, Phys. Rev. B **74**, 035101 (2006).

[47] B. Lee, L.-W. Wang, C. D. Spataru, and S. G. Louie, Nonlocal exchange correlation in screened-exchange density functional methods, Phys. Rev. B **76**, 245114 (2007).

[48] L.-W. Wang, Charging effects in a CdSe nanotetrapod, J. Phys. Chem. B **109**, 23330 (2005).

[49] N. E. Christensen, Electronic structure of GaAs under strain, Phys. Rev. B **30**, 5753 (1984).

[50] L.-W. Wang, Large-scale local-density-approximation band gap-corrected GaAsN calculations, Appl. Phys. Lett. **78**, 1565 (2001).

[51] S.-H. Wei, X. Nie, I. G. Batyrev, and S. B. Zhang, Breakdown of the band-gap-common-cation rule: The origin of the small band gap of InN, Phys. Rev. B **67**, 165209 (2003).

[52] S. Lany and A. Zunger, Generalized Koopmans density functional calculations reveal the deep acceptor state of N_O in ZnO, Phys. Rev. B **81**, 205209 (2010).

[53] W. Chen and A. Pasquarello, Band-edge levels in semiconductors and insulators: Hybrid density functional theory versus many-body perturbation theory, Phys. Rev. B **86**, 035134 (2012).

[54] W. Chen and A. Pasquarello, Accuracy of GW for calculating defect energy levels in solids, Phys. Rev. B **96**, 020101 (2017).

[55] D. K. Lewis, M. Matsubara, E. Bellotti, and S. Sharifzadeh, Quasiparticle and hybrid density functional methods in defect studies: An application to the nitrogen vacancy in GaN, Phys. Rev. B **96**, 235203 (2017).

[56] H. Kawanishi and Y. Hayafuji, A formation mechanism of X level due to an indium-carbon dimer in silicon, Adv. Mater. Res. **502**, 154 (2012).

[57] S. T. Pantelides, The electronic structure of impurities and other point defects in semiconductors, Rev. Mod. Phys. **50**, 797 (1978).

[58] M. He, X. Zhang, J. Huang, J. Li, C. Yan, J. Kim, Y.-S. Chen, L. Yang, J. M. Cairney, Y. Zhang, S. Chen, J. Kim, M. A. Green, and X. Hao, High efficiency $Cu_2ZnSn(S, Se)_4$ solar cells with shallow Li_{Zn} acceptor defects enabled by solution-based Li post-deposition treatment, Adv. Energy Mater. **11**, 2003783 (2021).

[59] B. Liu, J. Guo, R. Hao, L. Wang, K. Gu, S. Sun, and A. Aierken, Effect of Na doping on the performance and the band alignment of CZTS/CdS thin film solar cell, Solar Energy **201**, 219 (2020).

[60] A. Yamakata, J. J. M. Vequizo, T. Ogawa, K. Kato, S. Tsuboi, N. Furutani, M. Ohtsuka, S. Muto, A. Kuwabara, and Y. Sakata, Core-shell double doping of Zn and Ca on β-Ga_2O_3 photocatalysts for remarkable water splitting, ACS Catal. **11**, 1911 (2021).

[61] L. Liao, E. Kovalska, J. Luxa, L. Dekanovsky, V. Mazanek, L. Valdman, B. Wu, s. Huber, M. Mikulics, and Z. Sofer, Unraveling the mechanism of the persistent photoconductivity in InSe and its doped counterparts, Adv. Optic. Mater. **10**, 2200522 (2022).

[62] J. Jang, J.-K. Kim, J. Shin, J. Kim, K.-Y. Baek, J. Park, S. Park, Y. D. Kim, S. S. P. Parkin, K. Kang, K. Cho, and T. Lee, Reduced dopant-induced scattering in remote charge-transfer-doped MoS_2 field-effect transistors, Sci. Adv. **8**, eabn3181 (2022).

[63] T. Kamimura, Y. Nakata, M. H. Wong, and M. Higashiwaki, Normally-off Ga_2O_3 MOSFETs with unintentionally nitrogen-doped channel layer grown by plasma-assisted molecular beam epitaxy, IEEE Electron Device Lett. **40**, 1064 (2019).